Stabilization and Observation of Large-area Ferromagnetic Bimeron Lattice

Miming Cai,[1,2,*] Shangyuan Wang,[1,2,*] Yuelin Zhang,[1,2,*] Xiaoqing Bao,[1,2] Dekun Shen,[1,2] Jinghua Ren,[1,2] Lei Qiu[1,2], Haiming Yu[3], Zhenlin Luo[4], Mathias Kläui[5], Shilei Zhang[6], Nicolas Jaouen[7], Gerrit van der Laan[8], Thorsten Hesjedal[9], Ka Shen[1,2,10,†] and Jinxing Zhang[1,2,†]

[1]*School of Physics and Astronomy, Beijing Normal University, Beijing 100875, China.*

[2]*Key Laboratory of Multiscale Spin Physics, Ministry of Education, Beijing 100875, China.*

[3]*Fert Beijing Institute, MIIT Key Laboratory of Spintronics, School of Integrated Circuit Science and Engineering, Beihang University, Beijing 100191, China*

[4]*National Synchrotron Radiation Laboratory, University of Science and Technology of China, Hefei 230026, China.*

[5]*Institute of Physics, Johannes Gutenberg University Mainz, Staudinger Weg 7, Mainz 55128, Germany*

[6]*School of Physical Science and Technology, ShanghaiTech University, Shanghai 200031, China*

[7]*Synchrotron SOLEIL, L'Orme des Merisiers, 91192 Gif-sur-Yvette, France.*

[8]*Diamond Light Source, Harwell Science and Innovation Campus, Didcot OX11 0DE, UK.*

[9]*Department of Physics, University of Oxford, Oxford OX1 3PU, UK.*

[10]*The Center for Advanced Quantum Studies, Beijing Normal University, Beijing 100875, China*

*These authors contributed equally to this work.

†Correspondence to: kashen@bnu.edu.cn; jxzhang@bnu.edu.cn

Abstract

Symmetry engineering is an effective approach for generating emergent phases and quantum phenomena. In magnetic systems, the Dzyaloshinskii-Moriya (DM) interaction is essential for stabilizing chiral spin textures. The symmetry manipulation of DM vectors, described in three dimensions, could provide a strategy towards creating abundant topologically magnetic phases. Here, we have achieved to break the rotational and mirror symmetries of the three-dimensional DM vectors in a strongly correlated ferromagnet, which were directly measured through the non-reciprocal spin-wave propagations in both in-plane and out-of-plane magnetic field geometries. Combining cryogenic magnetic force microscopy and micromagnetic simulations, we discover a bimeron phase that emerges between spin spiral and skyrmion phases under an applied magnetic field. Such an artificially manipulated DM interaction is shown to play a critical role in the formation and evolution of the large-area bimeron lattice, a phenomenon that could be realized across a broad range of materials. Our findings demonstrate that symmetry engineering of the DM vectors can be practically achieved through epitaxial strain, paving the way for the creation of diverse spin topologies and the exploration of their emergent functionalities.

Exploration of topological spin textures in real space not only provides a platform to study the fundamental structures and emergent phenomena of solitons in physics [1-3], but also offers potential applications as ideal information units for beyond-CMOS logic and storage devices [4-6]. This has drawn significant attention from researchers across physics, materials science, and information technology [7-9]. Among these spin textures, magnetic skyrmions are particularly notable [10,11]. Their stabilization is largely governed by the Dzyaloshinskii-Moriya interaction (DMI) alongside the interplay of magnetocrystalline anisotropy, Zeeman energy, and magnetostatic energy. Since the discovery of DMI in ferromagnetic materials, systems that majorly exhibit interfacial-like [12,13] and bulk-like DMI [13-15] have been observed, which results in the formation of Néel-type and Bloch-type skyrmions as shown in Fig. 1(a) and 1(b), as well as merons [16-24], hopfions [25-27], chiral bobbers [28,29] and skyrmion strings[30,31], to name a few.

In physics, emergent phases or phenomena often arise when symmetry is reduced or broken [32]. In ferromagnets with DMI, the DM vectors can be described in the *x*-, *y*-, and *z*-directions of a three-dimensional Cartesian coordinate system [33], so that the elements and operations of crystal symmetry can therefore be used to describe the symmetry of the DMI [34,35]. In the majority of cases, the DM vectors that generate the topological spin textures [9,10,14-29] adhere to a relatively high degree of symmetry. A natural question arises: can reducing or breaking the symmetry of the DM vectors create opportunities for novel topological variants in magnets? In 2006,

Bogdanov *et al.* predicted that lower symmetry of DM vectors may bring about more non-trivial spin configurations [34]. Recent experiments have further suggested that reducing symmetry of DM vectors (i.e., anisotropic DMI) may stabilize exotic spin textures such as antiskyrmions [36-38]. Theoretical studies reveal that DM vectors without rotational and mirror symmetries could also give rise to the emergent topological magnetic textures such as bimeron as shown in Fig. 1(c), which may possess extraordinary dynamic properties under excitation compared to classical skyrmions [33,39]. Therefore, manipulating the symmetry of DM vectors may thus open the door to a much richer variety of spin topologies, as summarized in Fig. S1 and Table SI (for detail see Supplementary Information Section S2 [40]).

Despite the theoretical interests in stabilizing topological variants such as bimeron lattices through controllable symmetry of DM vectors in three dimensions, experimental realization still remains a challenge. Recently, Zhang *et al.* demonstrated that graded strain can effectively break the spatial inversion symmetry of crystals [41], which brings about a hybrid DMI in three dimensions and offers the possibility of engineering the desired symmetry of DM vectors. In this study, we show that DM vectors without rotational (C_n) and mirror (σ) symmetries can be artificially designed in a ferromagnetic oxide thin film, (La,Sr)MnO_3 (LSMO). Such a DMI are formed by the flexoresponse of the magnetic order with the strain gradient [42]. We directly observe the formation and evolution of a large-area bimeron lattice under varying external magnetic field, tracking its emergence from a spin spiral and its subsequent

transformation into a skyrmion lattice.

In general, the DM vectors of magnetic materials can be described by the following tensor (1) [41]

$$\boldsymbol{D} = \begin{bmatrix} \boldsymbol{D}_x \\ \boldsymbol{D}_y \\ \boldsymbol{D}_z \end{bmatrix} = \begin{bmatrix} D_{xx} & D_{xy} & D_{xz} \\ D_{yx} & D_{yy} & D_{yz} \\ D_{zx} & D_{zy} & D_{zz} \end{bmatrix} \quad (1)$$

where D_{ij} with $i = x, y, z$ represents the *j*th component of the DM vector for the spin pairs along [100], [010], and [001] axes, respectively. In the case of non-uniform strain, $D_{ij} = \nu_{ijmlk} E_{ml,k}$ where ν_{ijmlk} are the corresponding flexo-responsive coefficients of the strain-gradient components $E_{ml,k}$. Apart from the conventional DM components in the interfacial-like and bulk-like DMI (D_{xx}, D_{yy}, D_{zz}, D_{xy}, D_{yx}), the existence of *z*-components (D_{xz}, D_{yz}, D_{zx}, D_{zy}) is essential for achieving complete control over the symmetry of DM vectors in three dimensions. This provides a strong motivation to experimentally explore the configuration of DM components within the LSMO films and further deterministically control the symmetry of DM vectors by modulating epitaxial strain. For this purpose, a high-quality LSMO film with a strain relaxation and thickness of ~150 nm was epitaxially grown on $NdGaO_3$ as shown in Figs. S2 and S3 (for structural and magnetic characterization details see Supplementary Information Section S3 [40]).

The nonreciprocity of spin-wave propagation is usually used as an identification of the existence and amplitude of DMI [43-47]. In order to evaluate in-plane and out-of-plane DM components in LSMO film with a graded strain, spin-wave propagation

in a fully in-plane and out-of-plane magnetized LSMO film was characterized using a vector network analyzer in combination with a microwave probe (Supplementary Information Section S1 and S4 [40]). The detailed geometries for measuring the in-plane (D_{yx}) and out-of-plane (D_{xz}) components are illustrated in Figs. 2 and S4 [40]. For the former, the propagating spin wave along the *y*-axis was measured under magnetic saturation along the *x*-axis (also called Damon-Eshbach, DE mode). With an applied in-plane field of $\mu_0 H_{\text{ext}}$ = 140 mT [Fig. 2(a)], frequency nonreciprocity of $\delta f_{yx}(k) = f_{\text{DE}}(+k) - f_{\text{DE}}(-k) \approx -0.06$ GHz ($\mathbf{H} \parallel x$) is observed [Fig. 2(c)], which is proportional to D_{yx} according to the equation (2)

$$f_{\text{DE}}(\pm k, H_{\text{ext}}) = \frac{\gamma\mu_0}{2\pi}\sqrt{(Jk^2 - \xi + H_{\text{ext}} + M_{\text{s}})(Jk^2 + \xi + H_{\text{ext}})} \mp \frac{\gamma k}{\pi M_{\text{s}}} D_{\text{yx}} \qquad (2)$$

where $J = 2A/\mu_0 M_{\text{s}}$ and $\xi = M_{\text{s}}\left(1 - e^{-2|k|d}\right)/4$ with A being the exchange constant, M_{s} the saturation magnetization, μ_0 the vacuum permeability, γ the gyromagnetic ratio, d the thickness, k the wave vector, and H_{ext} the external field. The value of the in-plane DM component $D_{yx} = 1.41\times10^{-4}$ J m^{-2} is estimated by using the material parameters and $k = 2.07$ rad μm^{-1}.

Furthermore, the out-of-plane DM component D_{xz} can also lead to a frequency nonreciprocity in the magnetostatic forward volume (FV) spin waves. Therefore, we extend our non-local measurement to the FV modes. To the best of our knowledge, this has remained unexplored due to the absence of materials systems that exhibit an out-of-plane D_{xz} component. The experimental setup has been designed with an electromagnet that can be rotated axially to provide a magnetic vector field. The

propagating spin wave along the *x*-axis is then measured under magnetic saturation along the *z*-axis in an out-of-plane magnetic field, as shown in Fig. 2(b). During the measurement, the external magnetic field $\mu_0 H_{\mathrm{ext}}$ = 550 mT is applied along the *z*-axis for magnetic saturation. The magnetic hysteresis loop can be found in Fig. S3. A frequency nonreciprocity $\delta f_{xz} = f_{\mathrm{FV}}(+k) - f_{\mathrm{FV}}(-k) \approx 0.04$ GHz is observed [Fig. 2(d)]. The D_{xz} component is estimated though equation (3) [48]

$$f_{\mathrm{FV}}(\pm k, H_{\mathrm{ext}}) = \frac{\gamma\mu_0}{2\pi}\sqrt{(Jk^2 + \zeta + H_{\mathrm{ext}} + M_{\mathrm{eff}})(Jk^2 + H_{\mathrm{ext}} + M_{\mathrm{eff}})} \mp \frac{\gamma k}{\pi M_{\mathrm{s}}} D_{\mathrm{xz}} \quad (3)$$

where $\zeta = M_{\mathrm{s}}[1 - (1 - e^{-kd})/kd]$, $M_{\mathrm{eff}} = \mu_0 H_{\mathrm{ani}} - \mu_0 M_{\mathrm{s}}$,and $\mu_0 H_{\mathrm{ani}}$ is the perpendicular anisotropy field. $D_{xz} = -0.94\times10^{-4}$ J m^{-2} is estimated for the out-of-plane DM component. The spin-wave dispersion of FV modes was further simulated, as shown in Fig. S5, which confirms that this frequency nonreciprocity originates from the D_{xz} components. More details of the exploration of additional DM components can be found in Fig. S6 [40]. The comparable values of the in-plane and out-of-plane DM components clearly reveal a symmetry configuration of DM vectors in the LSMO film, e.g. a breaking of rotational (C_{n}) and mirror (σ) symmetries of the DM vectors as illustrated in Fig. 1(c) [33]. Such a DM configuration therefore provides an ideal platform for stabilizing more emergent topological magnetic textures.

To investigate the possible existence of emergent topological magnetic phases and their evolutions in real space, we employed cryogenic magnetic force microscopy (MFM) to image the magnetic domains under varying external magnetic fields (for detail see Supplementary Information Section S1 [40]). At 3.6 K, a spin spiral state,

confirmed by sinusoidal profile of the MFM phase (Fig. S8) [49], was observed in the absence of an applied magnetic field, as shown in the top panel of Fig. 3(a). The intensity of the MFM signal along the dashed path is plotted in the middle panel. It shows the same spiral characteristic as observed at room temperature, exhibiting an excellent periodicity over a large area. This periodicity has been characterized by MFM and resonant elastic x-ray scattering (REXS) and is shown in Fig. S7 [40]. When a magnetic field over -0.12 T was applied perpendicular to the film surface, a decrease in the intensity of MFM contrast was observed, suggesting a reduction of the local out-of-plane magnetization and an appearance of an "intermediate" spiral state as displayed in Fig. S9 [40]. When a perpendicular magnetic field of -0.3 T was applied, the "intermediate" spin spiral phase forms completely [Fig. 3(b)]. Both spiral states share a similar periodicity as confirmed by Fast Fourier Transform (FFT) analysis, as shown in the bottom panels of Fig. 3(a) and 3(b).

When the applied field strength exceeds -0.4 T, an unexpected magnetic phase emerges, characterized by pairs of semicircles with reversed out-of-plane magnetization cores, completely forming as a triangular arrangement [Fig. 3(c)]. Further increasing the external magnetic field strength to -0.465 T results in a transition to the skyrmion phase [Fig. 3(d)]. Notably, the FFT pattern of this emergent magnetic phase displays a distorted hexagonal periodicity, corresponding the arrangement in real space, as shown in dashed circles in the top panel of Fig. 3(c). It is distinct from the symmetric hexagonal periodicity characteristic of the skyrmion phase, as shown in the

bottom panels of Fig. 3(c) and 3(d). This lattice of paired semicircles, exhibiting a periodic arrangement, is an emergent phase rarely observed in magnets with traditional DMI [11,50]. The detailed evolution, including an analysis of the corresponding magnetic structures and periodicities as a function of magnetic field, is presented in Fig. S10 [40].

To better understand the nature and origin of the emergent magnetic phase with reversed cores and associated chirality, micromagnetic simulations were conducted. For the simulations, the DM vectors with both out-of-plane and in-plane components like Fig. 1(c) were assumed [33]. The magnetic textures were simulated using MUMAX3[51] with the out-of-plane DM component taken into account [33]. The value of the parameters adopted in the simulation can be found in the Supplementary Information Section S1 [40]. As plotted in Fig. 4, all the experimentally observed phases are reproduced. The comparison between simulated results in Fig. 4(a) and 4(b) suggests that the transition of the both spiral states as observed in Fig. 3(a) and 3(b), corresponding to the relative shrinking of two up/down magnetized domains under the perpendicular magnetic field. For the emergent phase with paired semicircles, the magnetization distribution of each bi-core unit exhibits a spin texture consistent to that of the predicted ferromagnetic bimeron [33]. The ferromagnetic bimeron lattice will further evolve into the magnetic skyrmion phase at increased magnetic fields. As shown in Fig. 4(c) and 4(d), the number of bimerons is equal to that of skyrmions, indicating the one-by-one transformation between these two topological spin textures. The spin

configuration at the top layer is shown in Fig. 4(a)-(d) bottom panel. Those at the middle and bottom layers are shown in Fig. S11. Thus, the detailed magnetization distribution of the observed bimeron lattice is further analyzed. Figure 4(f) reveals the combination of two specific chirality along the *x*- and *y*-axes in a bimeron as illustrated in Fig. 4(e), induced by the in-plane and out-of-plane DM components, i.e., D_{yx} and D_{xz}, respectively.

It is also noteworthy that, simulations with only interfacial DMI or without any DMI cannot be the case in the present observation, as shown in Fig. S12. With this, we conclude that the bimeron phase are driven by the three-dimensional DM vectors. This symmetry engineering of DM vectors facilitates the large-area stabilization of the bimeron lattice observed experimentally as shown in Fig. S13 [40]. The temperature-magnetic-field phase diagram [Fig. S14], which captures intermediate states, provides critical insights into understanding this transition and filling a previously unexplored gap in the exploration of the bimeron phase that occurs between spiral and skyrmion states. Our findings propose a practical strategy for tailoring magnetic textures by designing and controlling symmetry of DM vectors. Graded strain offers a precise method for engineering them via the interplay of crystal structure (e.g., rhombohedral, tetragonal, orthorhombic, monoclinic) and the strain configuration (e.g., tensile, compressive, and shear strain, and their relaxations)[41,42]. A deterministic control of the lattice, such as the relaxation of shear strain or anisotropic biaxial strain, may independently break the rotational or mirror symmetry of the DM vectors and generate

further variants of magnetic textures. This approach may extend beyond bimerons and skyrmions to a broader spectrum of magnetic phases, enabling the on-demand design of topological magnetic textures.

Conclusions

In summary, a three-dimensional configuration of DM vectors, breaking rotational and mirror symmetries, was artificially designed in a strain-graded LSMO thin film. This was quantitatively characterized by the frequency non-reciprocity of the spin-wave propagation. Such a DM configuration facilitated the stabilization of a large-area ferromagnetic bimeron lattice, which was directly observed during the phase evolution from a spin spiral to skyrmion state. Micromagnetic simulations highlighted the crucial role of the DM configuration with both out-of-plane and in-plane DM components in shaping this emergent topological spin texture. Our results demonstrate that artificially designed symmetry of DM vectors and its associated topological variants can be extended to a wide range of materials. The large-area bimeron phase observed in this strongly correlated oxide provides a novel platform for exploring emergent functionalities and quantum phenomena in both ground and excited states.

Acknowledgements

This work was supported by the National Natural Science Foundation (NSFC) of China (grant no. 52225205, J.Z.), the National Key Research and Development Program of China (grant no. 2023YFA1406500, J.Z. and grant no. 2021YFA0718700, J.Z.) and the Fundamental Research Funds for the Central Universities (J.Z., K.S. and Y.Z.). We also acknowledge the support of the NSFC (grants nos. T2350005, J.Z.; 11974047, K.S.; 12374100, K.S.; 12404119, Y.Z.), the Beijing Natural Science Foundation (Z240008, J.Z.) and the National Key R&D Program of China (grant no. 2022YFA1402801, H.Y.). The group in Mainz acknowledges support by the Deutsche Forschungsgemeinschaft (DFG, German Research Foundation) projects 403502522 (SPP 2137 Skyrmionics), 49741853, and 268565370 (SFB TRR173 projects A01, B02 and A12) as well as TopDyn. The work is a highly interactive collaboration supported by the Horizon 2020 Framework Program of the European Commission under ERC-2019-SyG no. 856538 (3D MAGiC) and the Horizon Europe project no. 101070290 (NIMFEIA).

Author contributions

M.C., Y.Z. and J.Z. conceived and designed the experiments. D.S. and J.R. were responsible for the thin film fabrication. M.C., Z.L., performed structural and magnetic characterization. M.C. and X.B. performed magnetic force microscopy. M.C., D.S., Y.Z. and H.Y. designed and fabricated the CPWs and performed the spin-wave propagation measurements. S.W., L.Q. and K.S. performed the micromagnetic simulation. S.Z., M.K. and N.J. were responsible for the designs or measurements of resonant elastic x-ray scattering. J.Z. supervised the experimental study, and H.Y., M.K., N.J., G.L. and T.H. provided related discussion. K.S. supervised the theoretical and simulated study. M.C., S.W., Y.Z., K.S. and J.Z. wrote the paper. M.K., S.Z., N.J., G.L. and T.H. contributed to the revision.

References

[1] L. Brey, H. A. Fertig, R. Côté, and A. H. MacDonald, Phys. Rev. Lett. **75**, 2562 (1995).

[2] U. Al Khawaja and H. Stoof, Nature **411**, 918 (2001).

[3] A. N. Bogdanov, U. K. Rößler, M. Wolf, and K. H. Müller, Phys. Rev. B **66**, 214410 (2002).

[4] J. Iwasaki, M. Mochizuki, and N. Nagaosa, Nat. Nanotechnol. **8**, 742 (2013).

[5] W. Jiang *et al.*, Science **349**, 283 (2015).

[6] O. Lee, R. Msiska, M. A. Brems, M. Kläui, H. Kurebayashi, and K. Everschor-Sitte, Appl. Phys. Lett. **122**, 260501 (2023).

[7] A. Fert, N. Reyren, and V. Cros, Nat. Rev. Mater. **2**, 17031 (2017).

[8] C. Back *et al.*, J. Phys. D: Appl. Phys. **53**, 363001 (2020).

[9] B. Göbel, I. Mertig, and O. A. Tretiakov, Phys. Rep. **895**, 1 (2021).

[10] S. Mühlbauer, B. Binz, F. Jonietz, C. Pfleiderer, A. Rosch, A. Neubauer, R. Georgii, and P. Böni, Science **323**, 915 (2009).

[11] X. Z. Yu, Y. Onose, N. Kanazawa, J. H. Park, J. H. Han, Y. Matsui, N. Nagaosa, and Y. Tokura, Nature **465**, 901 (2010).

[12] P. M. Levy and A. Fert, Phys. Rev. B **23**, 4667 (1981).

[13] A. R. Fert, Mater. Sci. Forum **59-60**, 439 (1991).

[14] A. Bogdanov and A. Hubert, J. Magn. Magn. Mater. **138**, 255 (1994).

[15] S. Seki, X. Z. Yu, S. Ishiwata, and Y. Tokura, Science **336**, 198 (2012).

[16] T. Shinjo, T. Okuno, R. Hassdorf, K. Shigeto, and T. Ono, Science **289**, 930 (2000).

[17] R. Hertel, S. Gliga, M. Fähnle, and C. M. Schneider, Phys. Rev. Lett. **98**, 117201 (2007).

[18] M. Curcic *et al.*, Phys. Rev. Lett. **101**, 197204 (2008).

[19] C. Phatak, A. K. Petford-Long, and O. Heinonen, Phys. Rev. Lett. **108**, 067205 (2012).

[20] S. Wintz *et al.*, Phys. Rev. Lett. **110**, 177201 (2013).

[21] S.-Z. Lin, A. Saxena, and C. D. Batista, Phys. Rev. B **91**, 224407 (2015).

[22] A. Nych, J.-i. Fukuda, U. Ognysta, S. Žumer, and I. Muševič, Nat. Phys. **13**, 1215 (2017).

[23] X. Z. Yu, W. Koshibae, Y. Tokunaga, K. Shibata, Y. Taguchi, N. Nagaosa, and Y. Tokura, Nature **564**, 95 (2018).

[24] M. Bhukta *et al.*, Nat. Commun. **15**, 1641 (2024).

[25] N. Kent *et al.*, Nat. Commun. **12**, 1562 (2021).

[26] D. Raftrey and P. Fischer, Phys. Rev. Lett. **127**, 257201 (2021).

[27] F. Zheng, N. S. Kiselev, F. N. Rybakov, L. Yang, W. Shi, S. Blügel, and R. E. Dunin-Borkowski, Nature **623**, 718 (2023).

[28] K. Ran, Y. Liu, Y. Guang, D. M. Burn, G. van der Laan, T. Hesjedal, H. Du, G. Yu, and S. Zhang, Phys. Rev. Lett. **126**, 017204 (2021).

[29] F. Zheng *et al.*, Nat. Nanotechnol. **13**, 451 (2018).

[30] M. T. Birch *et al.*, Nat. Commun. **13**, 3630 (2022).

[31] H. Jin *et al.*, Nano Lett. **23**, 5164 (2023).

[32] P. W. Anderson, Science **177**, 393 (1972).

[33] B. Göbel, A. Mook, J. Henk, I. Mertig, and O. A. Tretiakov, Phys. Rev. B **99**, 060407(R) (2019).

[34] U. K. Rößler, A. N. Bogdanov, and C. Pfleiderer, Nature **442**, 797 (2006).

[35] H. Niu *et al.*, Nat. Commun. **15**, 10199 (2024).

[36] K. Karube, L. Peng, J. Masell, X. Yu, F. Kagawa, Y. Tokura, and Y. Taguchi, Nat. Mater. **20**,

335 (2021).
[37] F. Zheng, N. S. Kiselev, L. Yang, V. M. Kuchkin, F. N. Rybakov, S. Blügel, and R. E. Dunin-Borkowski, Nat. Phys. **18**, 863 (2022).
[38] Z. He *et al.*, Nat. Mater. **23**, 1048 (2024).
[39] D. Yu, Y. Ga, P. Li, J. Jiang, J. Liang, L. Wang, C. Jia, K. Chang, and H. Yang, Phys. Rev. Lett. **133**, 206701 (2024).
[40] See Supplemental Material at [URL] for Section S1: method; Section S2: diverse symmetries of DM configurations and related magnetic textures; Section S3: structural and magnetic characterizations; Section S4: nonreciprocal spin-wave spectra; Section S5: MFM image and REXS characterization of the ground state magnetic order; Section S6: MFM analysis of the evolution of the magnetic textures; Section S7: micromagnetic simulations of magnetic structures; Section S8: large-area stabilization of bimeron lattice and the detailed phase diagram.
[41] Y. Zhang *et al.*, Phys. Rev. Lett. **127**, 117204 (2021).
[42] D. A. Kitchaev, I. J. Beyerlein, and A. Van der Ven, Phys. Rev. B **98**, 214414 (2018).
[43] S. Seki *et al.*, Phys. Rev. B **93**, 235131 (2016).
[44] J. M. Lee, C. Jang, B.-C. Min, S.-W. Lee, K.-J. Lee, and J. Chang, Nano Lett. **16**, 62 (2015).
[45] J. Cho *et al.*, Nat. Commun. **6**, 7635 (2015).
[46] H. T. Nembach, J. M. Shaw, M. Weiler, E. Jué, and T. J. Silva, Nat. Phys. **11**, 825 (2015).
[47] K. Zakeri, Y. Zhang, J. Prokop, T. H. Chuang, N. Sakr, W. X. Tang, and J. Kirschner, Phys. Rev. Lett. **104**, 137203 (2010).
[48] A. Prabhakar and D. D. Stancil, *Spin waves: Theory and applications* (Springer, 2009), Vol. 5.
[49] W. Legrand, D. Maccariello, F. Ajejas, S. Collin, A. Vecchiola, K. Bouzehouane, N. Reyren, V. Cros, and A. Fert, Nat. Mater. **19**, 34 (2019).
[50] C. Jin *et al.*, Nat. Commun. **8**, 15569 (2017).
[51] A. Vansteenkiste, J. Leliaert, M. Dvornik, M. Helsen, F. Garcia-Sanchez, and B. Van Waeyenberge, AIP Adv. **4**, 107133 (2014).

Figures

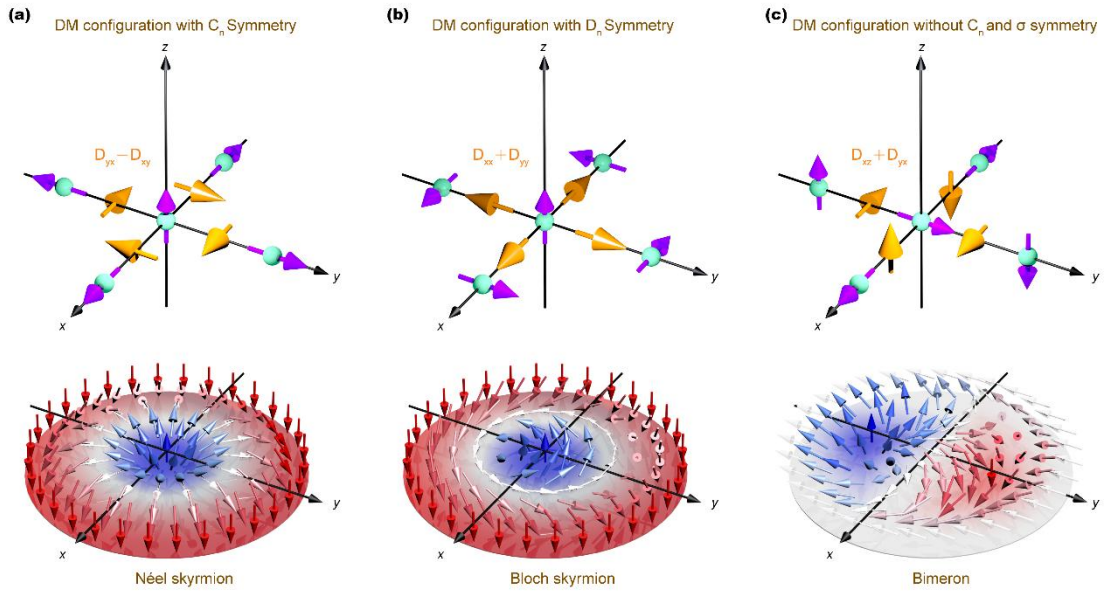

FIG. 1. DM configurations with different symmetries and corresponding energy-preferred topological spin textures. (a), (b) Classical DM configurations with rotational (C_n) or mirror (σ) symmetries and corresponding energetically stabilized Néel and Bloch-type skyrmions, respectively. **(c)** Three-dimensional DM configuration without C_n and σ symmetries and its associated bimeron state. Schematics of DM vector distributions are shown in the top panels and the detailed magnetic textures are depicted in the bottom panels.

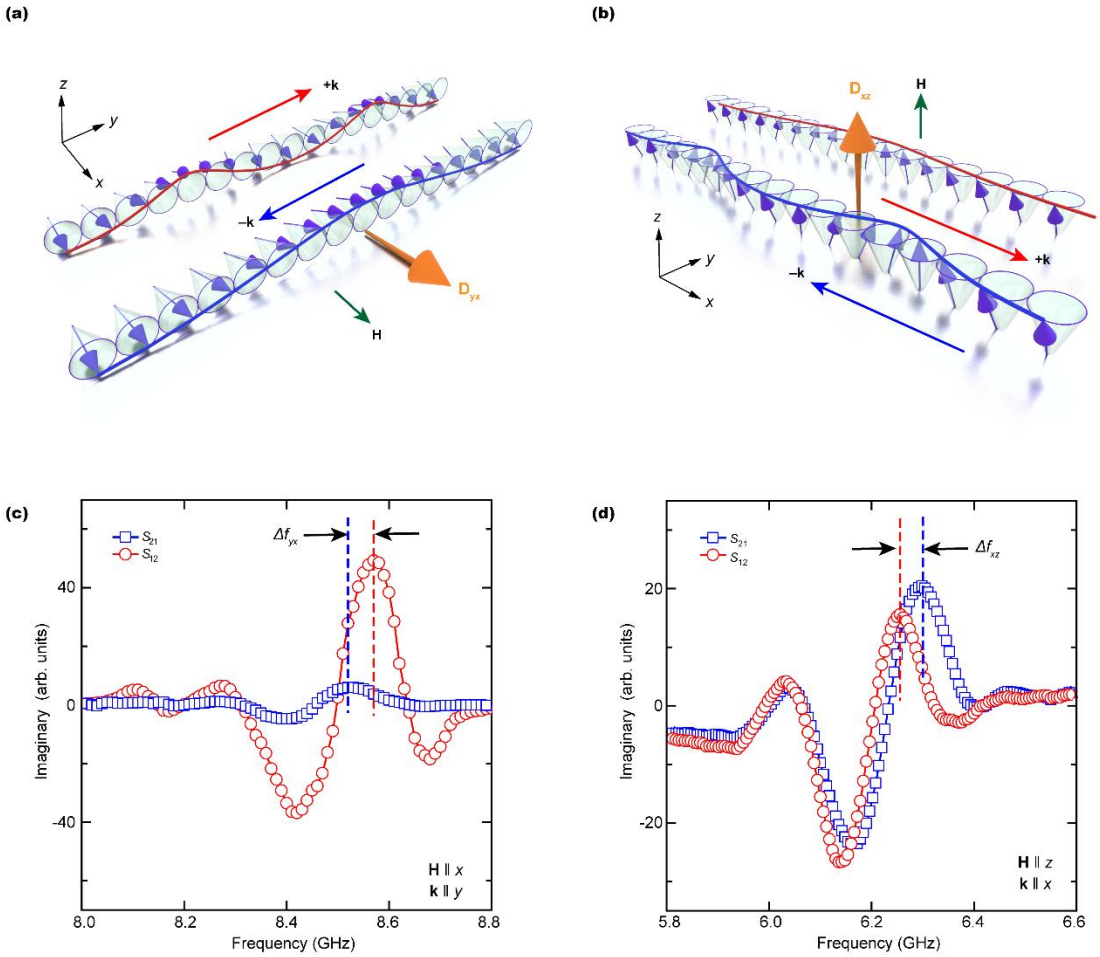

FIG. 2. Coexisting spin-wave frequency nonreciprocities induced by in-plane and out-of-plane DM components. (a), (b) Schematics of in-plane and out-of-plane DM vectors and their corresponding nonreciprocal spin-wave propagation, respectively. The DM component D_{yx} and D_{xz} are shown by orange arrows. The corresponding spin-wave vector $\pm\mathbf{k}$ (blue and red arrows) aligns along the y-axis (x-axis), and the external magnetic field $\mathbf{H}$ (green arrows) aligns along the x-axis (z-axis), respectively. **(c), (d)** Experimental transmission spectra of nonreciprocal spin-wave propagation at room temperature under $\mathbf{H} \parallel x$ and $\mathbf{H} \parallel z$ configurations, respectively. Spin waves in the transmission spectrum S_{21} ($+\mathbf{k}$) propagate from coplanar waveguide 1 (CPW1) to CPW2, while the S_{12} ($-\mathbf{k}$) spectrum describes propagation in the reverse direction.

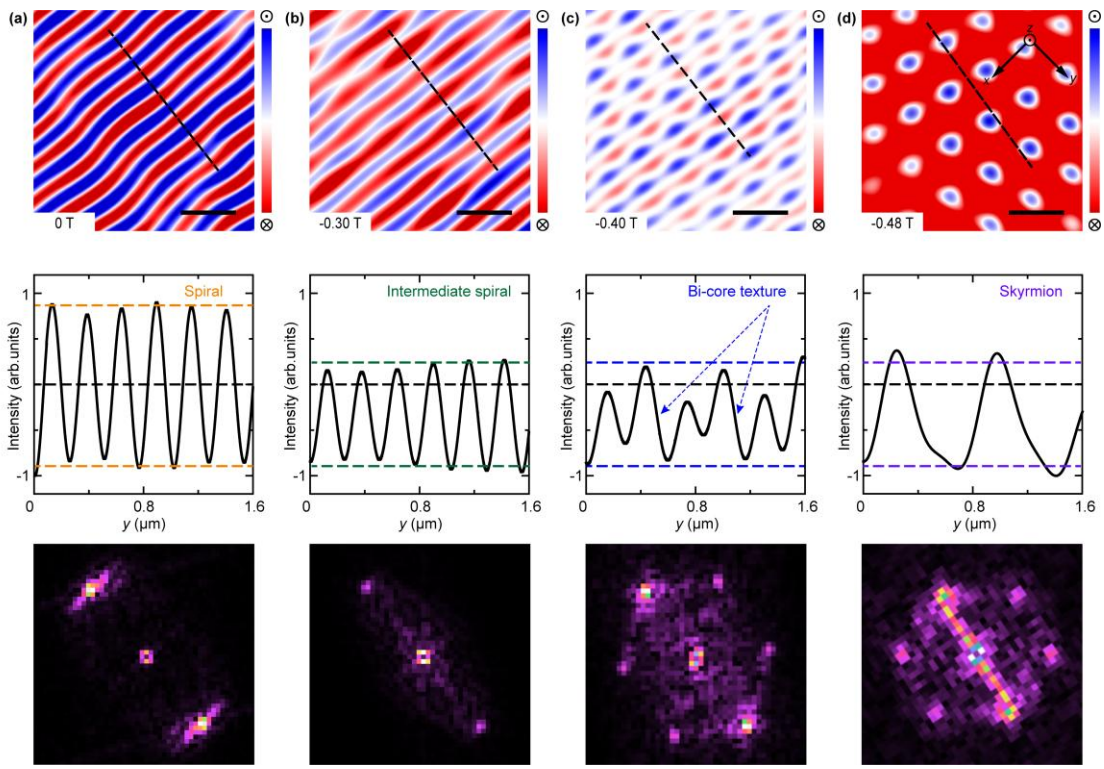

FIG. 3. Field-dependent evolution of spin textures. (a)-(d) Real-space images of spin textures under varying out-of-plane external fields (z-axis), captured by magnetic force microscopy (MFM) imaging (top panel). The dashed circles highlight the periodicity of the bi-core lattice. All scale bars represent 500 nm. The middle panels show line plots along the y-axis, as indicated by the respective dashed lines above. The normalized stray field intensity from the local magnetization highlights the intensity differences between the spiral phase, intermediate spiral, bi-core, and skyrmion phase. The FFT patterns of the different magnetic textures, which illustrate their periodicities, are displayed in the bottom panels.

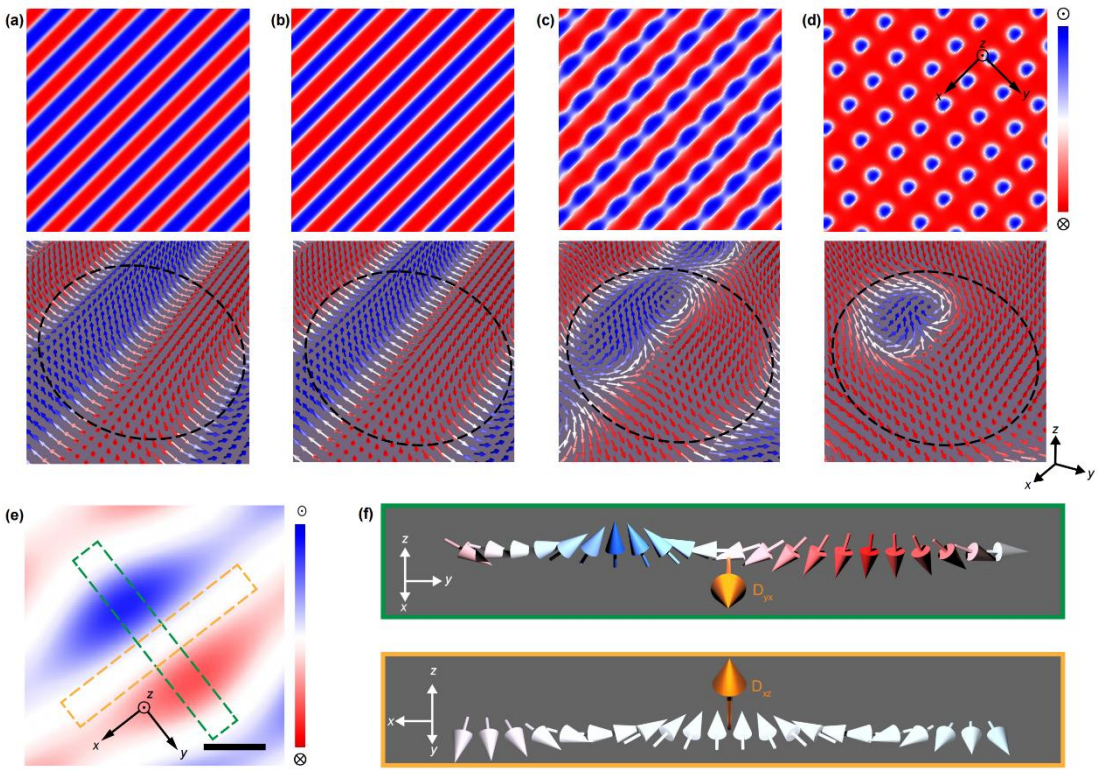

FIG. 4. The appearance of ferromagnetic bimeron lattice driven by in-plane and out-of-plane DM vectors. (a)-(d) The simulated lattice states of spiral, intermediate spiral, bimeron and skyrmion textures. Their corresponding spin arrangements at the top layer are presented in detail by colorful arrows at the bottom and the black circles point out the in-situ transformations of the above textures. **(e)** The unit of bimeron from experimental observation. Yellow and green boxes indicate that the chiralities of spin arrangements along the *x*- and *y*-axes are different. The scale bar is 250 nm. **(f)** The different spin chiralities in ferromagnetic bimeron. The spin arrangement along the *y*-axis (green box in e) is shown at the top and exhibits out-of-plane chirality, which is induced by the in-plane DM vector D_{yx}. In contrast, the spin arrangement along the *x*-axis (yellow box in e) is shown at the bottom and exhibits in-plane chirality, which is induced by the out-of-plane DM vector D_{xz}.